Chapter 1

Nuclear Reactions: Concepts and Cross Sections

> *"A nuclear reaction is a rearrangement of nucleons under the strong interaction. The cross section converts a microscopic probability into a measurable counting rate."*
>
> experimental nuclear physics [6, 1]

Radioactive decay is spontaneous. **Nuclear reactions** are induced: a projectile strikes a target and nucleons are redistributed. This chapter introduces the notation $a + A \to b + B$, the conservation laws that decide whether a channel is possible, and a dimensionally careful definition of differential and total cross sections. It then develops flux and luminosity, laboratory versus centre-of-mass (CM) energies, reaction types, and direct, pre-equilibrium, compound, and statistical mechanisms with their characteristic timescales and Bohr's independence hypothesis [6, 1, 14, 2].

1.1 General form of a nuclear reaction

A two-body reaction is written

$$a + A \longrightarrow b + B, \tag{1.1}$$

or in compact spectroscopic notation

$$A(a, b)B. \tag{1.2}$$

Here a is the **projectile**, A the **target**, b the detected light product, and B the **residual** (often left in the target). Examples: $^{14}\mathrm{N}(\alpha, p)^{17}\mathrm{O}$, $^{238}\mathrm{U}(n, \gamma)^{239}\mathrm{U}$. If several light particles emerge one writes $A(a, np)B$, and so on [6, 1].

1.1.1 Conservation laws as channel filters

Every proposed channel must conserve total energy, linear momentum, angular momentum, electric charge, and baryon (nucleon) number. For strong and electromagnetic reactions parity is also conserved; isospin is approximate because Coulomb and charge-dependent nuclear terms

break the symmetry. Thus

$$Z_a + Z_A = Z_b + Z_B, \qquad A_a + A_A = A_b + A_B, \tag{1.3}$$

$$P_a^\mu + P_A^\mu = P_b^\mu + P_B^\mu, \qquad \mathbf{J}_i = \mathbf{J}_f. \tag{1.4}$$

The four-momentum equation contains both energy and three-momentum conservation and is valid in every inertial frame. Charge and nucleon number are quick bookkeeping tests; four-momentum conservation supplies the Q-value and the kinematic restrictions developed in the next lecture. Lepton number must additionally be conserved when leptons occur in a weak reaction [6, 1, 14].

Decay versus reaction. In α or β decay a single parent rearranges spontaneously. In a reaction two nuclei interact because the experimenter supplies a beam (or a neutron flux). Gamma decay changes neither Z nor A; reactions generally do.

1.2 Experimental setup

A typical arrangement is:

(i) an accelerator (or radioactive source, or reactor) that produces a beam of projectiles a with known kinetic energy;

(ii) a thin target containing nuclei A, in vacuum to avoid air scattering;

(iii) one or more detectors that count product particles b in a solid angle $\mathrm{d}\Omega$ at laboratory angle θ, and measure their kinetic energy.

The residual B often stops in the target. The raw data are counts versus energy at each angle: the ingredients of a differential cross section [6, 1].

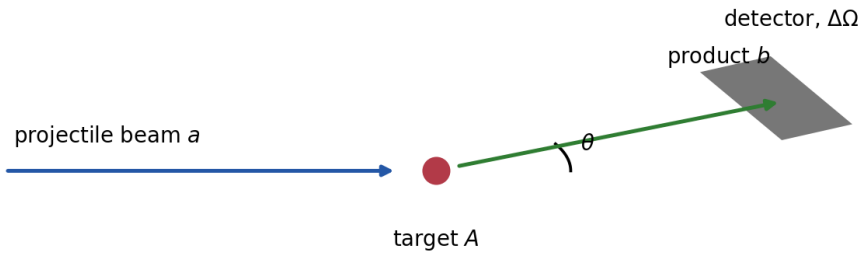

Figure 1.1: Schematic of a fixed-target scattering/reaction experiment: beam, target, and detector at angle θ subtending solid angle $\mathrm{d}\Omega$.

Heavy-ion beams open additional reaction mechanisms; this chapter focuses on light projectiles (n, p, d, α, …) [14, 2].

1.3 Definition of the cross section

1.3.1 Flux, luminosity, and counting rate

Let Φ be the incident **flux density**,

$$\Phi = \frac{\mathrm{d}N_a}{\mathrm{d}A\,\mathrm{d}t}, \tag{1.5}$$

in projectiles per unit area per unit time. If N_t target nuclei are illuminated uniformly, the differential reaction rate defines the **differential cross section**:

$$\mathrm{d}\dot{N} = \Phi N_t \frac{\mathrm{d}\sigma}{\mathrm{d}\Omega}\,\mathrm{d}\Omega, \qquad \frac{\mathrm{d}\sigma}{\mathrm{d}\Omega} = \frac{\mathrm{d}\dot{N}}{\Phi N_t\,\mathrm{d}\Omega}. \tag{1.6}$$

The partial cross section for channel c, and the sum over all nonelastic channels, are

$$\sigma_c = \int_{4\pi} \frac{\mathrm{d}\sigma_c}{\mathrm{d}\Omega}\,\mathrm{d}\Omega, \qquad \sigma_{\mathrm{reac}} = \sum_{c\neq\mathrm{elastic}} \sigma_c. \tag{1.7}$$

An inclusive cross section sums over unobserved final states; an exclusive cross section specifies them. These definitions prevent the common mistake of calling a count, a rate, and a cross section the same quantity.

Physical meaning. The cross section is an effective area: if every projectile that hits a disk of area σ centred on a target nucleus reacted, the observed rate would match experiment. It is not generally the geometrical area of a nucleus: interference and resonances can make it much smaller or much larger [6, 1, 14].

1.3.2 Areal density, luminosity, and attenuation

If a target has volume density n, thickness t, and illuminated area A', then

$$N_t = nA't = n_a A', \qquad n_a \equiv nt. \tag{1.8}$$

The beam rate is $\dot{N}_a = \Phi A'$. Their product gives the fixed-target **luminosity**,

$$\mathcal{L} = \dot{N}_a n_a, \qquad [\mathcal{L}] = \mathrm{area}^{-1}\mathrm{time}^{-1}, \tag{1.9}$$

and hence

$$N_{\mathrm{obs}} = T \int_{\Delta\Omega} \mathcal{L}\,\epsilon(\Omega)\frac{\mathrm{d}\sigma}{\mathrm{d}\Omega}\,\mathrm{d}\Omega. \tag{1.10}$$

Here T is live time and ϵ includes intrinsic efficiency, dead-time correction, and analysis acceptance. For nonuniform profiles, $\mathcal{L} = \int \Phi(x,y) n_a(x,y)\,\mathrm{d}A$.

For a thin target $P_{\mathrm{int}} \simeq n_a \sigma_{\mathrm{tot}}$. The exact attenuation law is

$$I(t) = I(0)e^{-n\sigma_{\mathrm{tot}}t}, \qquad P_{\mathrm{int}} = 1 - e^{-n\sigma_{\mathrm{tot}}t}. \tag{1.11}$$

For thick targets one must also integrate the energy-dependent cross section as the beam loses energy in the material [6, 1, 2].

1.3.3 Units: the barn

Because a rate equals luminosity times cross section, σ has units of **area**. Steradians are dimensionless, but "per sr" is retained to display the angular normalization of $\mathrm{d}\sigma/\mathrm{d}\Omega$. The practical nuclear unit is the barn:

$$1\,\mathrm{b} = 10^{-24}\,\mathrm{cm}^2 = 10^{-28}\,\mathrm{m}^2. \tag{1.12}$$

Typical reaction cross sections range from microbarns to thousands of barns (resonant neutron capture) [6, 1].

Remark

Rutherford scattering already used the same idea: $\mathrm{d}\sigma/\mathrm{d}\Omega$ is the quantity that multiplies flux and target density to give a counting rate. Nuclear reactions generalise that language to all exit channels [2, 14].

1.4 Laboratory and centre-of-mass frames

Theory is simplest in the **centre-of-mass (CM)** frame, where total momentum vanishes. In the laboratory the target is usually at rest. For non-relativistic two-body kinematics with projectile mass m_a, target mass m_A, and laboratory kinetic energy E_{lab},

$$E_{\mathrm{cm}} = \frac{m_A}{m_a + m_A}\,E_{\mathrm{lab}} = \frac{\mu}{m_a}\,E_{\mathrm{lab}}, \tag{1.13}$$

where $\mu = m_a m_A/(m_a + m_A)$ is the reduced mass. Derivation: the CM velocity in the lab is $v_{\mathrm{cm}} = m_a v_1/(m_a + m_A)$. In the CM frame the relative speed remains v_1, and

$$E_{\mathrm{cm}} = \tfrac{1}{2}\mu v_1^2 = \frac{m_A}{m_a + m_A}\left(\tfrac{1}{2} m_a v_1^2\right) = \frac{m_A}{m_a + m_A}\,E_{\mathrm{lab}}. \tag{1.14}$$

Only E_{cm} is available for excitation and reaction Q-value balance; the remainder is locked in CM motion of the system as a whole [6, 1].

The laboratory scattering angle θ_{lab} and CM angle θ_{cm} are related (elastic equal-mass special cases aside) by

$$\tan\theta_{\mathrm{lab}} = \frac{\sin\theta_{\mathrm{cm}}}{\cos\theta_{\mathrm{cm}} + m_a/m_A} \tag{1.15}$$

for elastic scattering of a on A (standard textbook form). Angular distributions should always state the frame [6, 14].

1.5 Coulomb barrier

For charged projectiles the long-range force is Coulomb repulsion. At separation r,

$$V_C(r) = \frac{1}{4\pi\varepsilon_0}\,\frac{Z_a Z_A e^2}{r}. \tag{1.16}$$

Near the nuclear surface $r \approx R_a + R_A \approx r_0(A_a^{1/3} + A_A^{1/3})$ the Coulomb barrier height is of order several MeV for light ions on medium targets, and tens of MeV for heavy systems. Below the barrier, elastic Coulomb (Rutherford) scattering dominates; nuclear reactions require penetration of the barrier (tunnelling) or energies above it. Neutrons feel no Coulomb barrier and can react at thermal energies [6, 1, 2].

At short distance the attractive nuclear potential takes over, producing a pocket that supports compound-nucleus resonances (next chapter and fission lectures).

1.6 Types of processes

1.6.1 Scattering versus reaction

If $a = b$ and $A = B$ as nuclear species, one speaks of **scattering**. If identities change ($a \neq b$ or $A \neq B$), one speaks of a **reaction** in the narrow sense. Both are nuclear reactions in the broad sense [6].

1.6.2 Elastic and inelastic scattering

Elastic scattering leaves A in its ground state. Total kinetic energy is conserved in the CM frame (rest masses unchanged):

$$K_a + K_A = K'_a + K'_A. \tag{1.17}$$

Inelastic scattering excites A (or a) by energy E^*:

$$K_a + K_A = K'_a + K'_A + E^*. \tag{1.18}$$

The detected spectrum shows discrete peaks at kinetic energies reduced by E^* (recoil corrected) [6, 1].

1.6.3 Transfer: stripping and pickup

In a **transfer reaction** one or more nucleons move between projectile and target.

- **Stripping:** the projectile loses a nucleon to the target. Example: (d, p) deposits a neutron; the proton is detected.
- **Pickup:** the projectile gains a nucleon from the target. Example: (p, d) picks up a neutron.

Transfer angular distributions are sensitive to the orbital angular momentum of the transferred nucleon and are a primary tool of nuclear spectroscopy [6, 14].

1.6.4 Capture

In a **capture reaction** the projectile is absorbed and the residual de-excites, often by γ emission: $A(n, \gamma)B$, $A(p, \gamma)B$. Neutron capture on heavy nuclei is central to reactors and nucleosynthesis [6, 1].

1.7 Direct, pre-equilibrium, and compound mechanisms

1.7.1 Timescales

Two limiting mechanisms organise most data:

(1) **Direct reactions.** The projectile interacts with one or a few surface nucleons and exits promptly. The characteristic time is the transit time across the nucleus,

$$t_{\rm direct} \sim \frac{2R}{v} \sim 10^{-22}\,\mathrm{s} \tag{1.19}$$

for $\sim 20\,\mathrm{MeV}$ nucleons ($v \sim 0.2c$, $R \sim 10\,\mathrm{fm}$). Angular distributions are **forward peaked**: memory of the beam direction survives.

(2) **Compound-nucleus (CN) reactions.** The projectile is absorbed; its energy is shared among many nucleons until a quasi-equilibrated excited nucleus C^* forms. A resolved compound level of total width Γ has mean life

$$\tau_{\rm CN} = \frac{\hbar}{\Gamma}. \tag{1.20}$$

Thus widths from $1\,\mathrm{MeV}$ down to $10^{-6}\,\mathrm{eV}$ correspond to $\tau \simeq 6.6\times10^{-22}$ up to $6.6\times10^{-10}\,\mathrm{s}$. There is no universal 10^{-16}–$10^{-15}\,\mathrm{s}$ compound lifetime: broad, overlapping resonances can be much shorter and isolated neutron resonances much longer. What distinguishes an equilibrated compound mechanism is the separation from the transit/equilibration time and the loss of detailed entrance-channel memory. Emission resembles evaporation; in the CM frame the angular distribution is nearly **symmetric** (often nearly isotropic for high level density) [6, 1, 14].

Real reactions can interpolate between these limits. In a **pre-equilibrium** reaction the projectile has undergone several collisions and shared part, but not all, of its energy before emission. Such spectra retain some forward memory while extending toward the softer, evaporation-like compound spectrum. Once equilibration is reached, a **statistical** description replaces individual many-body amplitudes by level densities and channel transmission coefficients. The Hauser–Feshbach cross section has the schematic factorisation

$$\sigma_{aA\to bB} \sim \sum_{J\pi} \sigma^{J\pi}_{\rm form}(aA)\,\frac{T^{J\pi}_{bB}}{\sum_c T^{J\pi}_c}, \tag{1.21}$$

with angular-momentum and parity conservation imposed in each J^π class. The numerator forms the compound state and the ratio is its branching probability. This is the quantitative statistical implementation of Bohr independence. The factorisation is valid after averaging over enough compound levels that formation and decay amplitudes decorrelate. Near thresholds, for low level density, for doorway states, or when direct and compound amplitudes interfere, a simple Hauser–Feshbach average can fail. Width-fluctuation corrections are also needed when entrance and exit channels remain correlated [6, 1].

Symbolically,

$$a + A \;\longrightarrow\; C^* \;\longrightarrow\; b + B. \tag{1.22}$$

1.7.2 de Broglie wavelength and energy regime

The projectile de Broglie wavelength (often quoted as the reduced wavelength $\bar{\lambda} = \hbar/p$) sets the spatial scale of the interaction:

$$\bar{\lambda} = \frac{\hbar}{p} = \frac{\hbar c}{\sqrt{2 m_a c^2 \, E}}. \tag{1.23}$$

Using $\hbar c \approx 197\,\mathrm{MeV}\cdot\mathrm{fm}$ and $m_p c^2 \approx 938\,\mathrm{MeV}$, a 10 MeV proton has

$$\bar{\lambda} \approx \frac{197}{\sqrt{2 \times 938 \times 10}} \approx \frac{197}{137} \approx 1.4\,\mathrm{fm}, \tag{1.24}$$

while the full wavelength $h/p = 2\pi\bar{\lambda}$ is a few fm, comparable to a medium nucleus and favourable to CN formation. At $E \sim 40\,\mathrm{MeV}$, $\bar{\lambda} \sim 0.7\,\mathrm{fm}$ approaches nucleon size and direct processes gain weight [6, 1].

1.7.3 Bohr independence hypothesis

Bohr's **independence hypothesis** states that once C^* is formed at a given excitation energy, spin, and parity, it forgets the entrance channel. Decay branching ratios depend only on the properties of C^*, not on whether C^* was made by $p + A$ or $\alpha + A'$.

Classic test: Ghoshal's experiment comparing

$$p + {}^{63}\mathrm{Cu} \to {}^{64}\mathrm{Zn}^* \to \text{various exit channels} \tag{1.25}$$

with

$$\alpha + {}^{60}\mathrm{Ni} \to {}^{64}\mathrm{Zn}^* \to \text{same exit channels}. \tag{1.26}$$

The comparison requires more than matching a laboratory energy: the two entrances must form the same ${}^{64}\mathrm{Zn}^*$ excitation interval and must populate comparable J^π ensembles (or the data must be averaged so that differences are removed). One then compares *decay branching patterns* after separating entrance-channel formation factors. Ghoshal found closely corresponding excitation-function structures for common exit channels, supporting compound-nucleus independence within those conditions; the absolute cross sections need not coincide [37, 6, 1].

Matching excitation energies. Absorption of a proton on stationary ${}^{63}\mathrm{Cu}$ forms ${}^{64}\mathrm{Zn}^*$ with excitation

$$\Delta E = (m_p + m_{\mathrm{Cu}} - m_{\mathrm{Zn}})c^2 + \frac{m_{\mathrm{Cu}}}{m_p + m_{\mathrm{Cu}}} K_p, \tag{1.27}$$

because only the CM kinetic energy is available internally. Therefore the laboratory energy needed for a chosen ΔE is

$$K_p = \left[\Delta E - (m_p + m_{\mathrm{Cu}} - m_{\mathrm{Zn}})c^2\right]\left(1 + \frac{m_p}{m_{\mathrm{Cu}}}\right). \tag{1.28}$$

An analogous formula with $(m_\alpha, m_{\mathrm{Ni}})$ replaces (m_p, m_{Cu}) for the α channel. Different mass combinations imply different laboratory energy scales for the same ΔE, which is why Ghoshal plots use two shifted energy axes [37, 6].

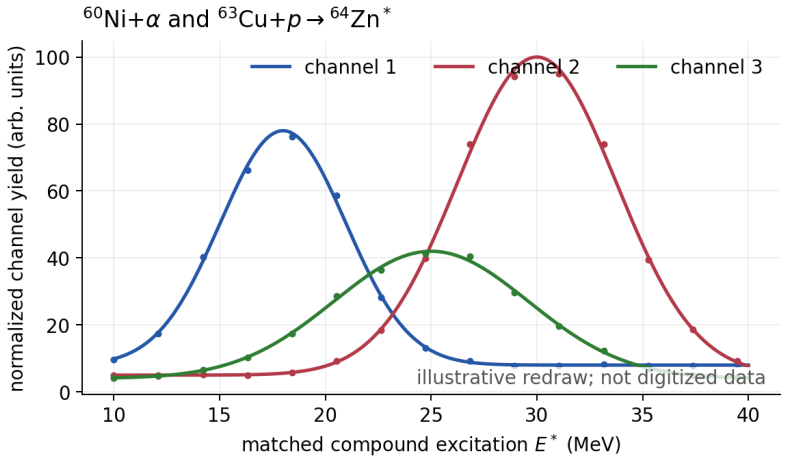

Figure 1.2: The same ^{64}Zn* compound system formed through $^{60}\mathrm{Ni} + \alpha$ and $^{63}\mathrm{Cu} + p$. Corresponding decay structures are compared only after matching compound excitation and accounting for the populated J^π distributions and formation normalizations. Redrawn schematic after Ghoshal; points are illustrative, not digitized data [37].

Bohr compound nucleus (1936)

Niels Bohr proposed that low-energy nuclear reactions proceed through a long-lived intermediate nucleus in statistical equilibrium. The picture explains dense resonances, nearly isotropic evaporation spectra, and entrance-channel independence. Direct reactions (Butler, Austern, ...) emerged later as the complementary short-timescale limit [6, 14, 2].

Key idea

Students should remember:

- Reaction: $a + A \to b + B$ or $A(a, b)B$.
- $\mathrm{d}\dot{N} = \Phi N_t(\mathrm{d}\sigma/\mathrm{d}\Omega)\mathrm{d}\Omega$, or $\dot{N} = \mathcal{L}\sigma$; counts require live time and efficiency.
- σ has units of area; $1\,\mathrm{b} = 10^{-24}\,\mathrm{cm}^2$.
- $E_{\mathrm{cm}} = m_A E_{\mathrm{lab}}/(m_a + m_A)$.
- Elastic vs inelastic; stripping/pickup; capture; Coulomb barrier for charged beams.
- Direct $\sim 10^{-22}\,\mathrm{s}$, forward peaked; pre-equilibrium interpolates; for a resolved CN level $\tau = \hbar/\Gamma$, with a broad range set by its width; statistical decay is more symmetric in the CM.

1.8 Deeper physics: direct versus compound reactions and geometric cross sections

1.8.1 Geometric cross section as a scale

When two nuclei collide, a useful order-of-magnitude target area is the geometric cross section

$$\sigma_{\mathrm{geom}} \approx \pi(R_1 + R_2)^2, \qquad R \approx r_0 A^{1/3}, \tag{1.29}$$

with $r_0 \approx 1.2\,\mathrm{fm}$ [6, 14]. Elastic and reaction cross sections at tens of MeV per nucleon often approach this scale when absorption is strong. The *reaction* cross section $\sigma_{\mathrm{reaction}}$ measures flux removed from the elastic channel; at high energy $\sigma_{\mathrm{reaction}} \lesssim \sigma_{\mathrm{geom}}$, while at low energy Coulomb repulsion suppresses both [6, 1].

Geometric estimate for $^{12}\mathrm{C} + ^{12}\mathrm{C}$

With $R \approx 1.2 \times 12^{1/3}\,\mathrm{fm} \approx 2.6\,\mathrm{fm}$ for each nucleus, $R_1 + R_2 \approx 5.2\,\mathrm{fm}$ and $\sigma_{\mathrm{geom}} \approx \pi(5.2\,\mathrm{fm})^2 \approx 85\,\mathrm{fm}^2 \approx 850\,\mathrm{mb}$ [6]. Measured fusion cross sections at barrier energies are smaller because tunneling and angular-momentum filtering reduce the effective area (Lecture 25).

1.8.2 Direct versus compound mechanisms

Direct reactions (stripping, pickup, knockout) transfer one or a few nucleons in a single encounter. Characteristic times are $\sim 10^{-22}\,\mathrm{s}$ (the transit time across a nuclear diameter). Angular distributions are strongly forward peaked and carry information about transferred ℓ [6, 14]. **Compound-nucleus (CN) reactions** form a long-lived equilibrated intermediate ($\sim 10^{-21}$ to $10^{-15}\,\mathrm{s}$). Decay is statistical: angular distributions are nearly isotropic in the CM frame, and outgoing energies follow an evaporation spectrum [6, 1].

Remark

The labels "direct" and "compound" are dynamical limits, not exclusive channels. The same final state can receive contributions from both mechanisms. Ghoshal's classic comparison of (p, p) and (p, n) on the same target illustrates how compound-nucleus averaging smooths excitation functions while direct channels retain angular structure [37, 6].

Key idea

Link to decay and fission. Direct reactions probe single-particle overlap (as in β and γ matrix elements). Compound-nucleus decay is the inelastic analogue of the statistical evaporation that follows fission or fusion (Lectures 22–24). The geometric cross section sets the flux scale; the mechanism determines how that flux is distributed in angle and energy [14, 2].

1.8.3 Lifetime scales and the Hauser–Feshbach limit

Direct reactions complete in $\sim R/v \sim 10^{-22}\,\mathrm{s}$. Compound-nucleus lifetimes range from $10^{-21}\,\mathrm{s}$ for light nuclei to $10^{-15}\,\mathrm{s}$ or longer for heavy systems near the fission barrier [6, 14]. The Weisskopf estimate for a single γ step is $\sim 10^{-13}\,\mathrm{s}$ for a MeV transition; a compound nucleus typically emits many γ rays before fission or particle emission, so the total CN lifetime is the sum of many statistical steps. Pre-equilibrium emission fills the gap between direct and compound time scales and produces forward-peaked continuum particles that are neither pure direct nor pure evaporation [6, 1].

1.8.4 Optical model and absorption

The complex optical potential used for elastic scattering has an imaginary part that removes flux from the elastic channel into reaction channels [6, 14]. The optical theorem relates the forward elastic amplitude to the total cross section, so a good optical-model fit to elastic data constrains the reaction cross section as well. DWBA calculations for transfer reactions use the same optical potentials to generate distorted waves; spectroscopic factors extracted from (d, p) cross sections therefore inherit optical-model uncertainties that modern analyses quote as covariance bands [51, 37]. This is the reaction-theory counterpart of hindrance factors in decay: the barrier or potential is known approximately, but the overlap integral is model dependent.

Geometric scale

For $R = 1.2(A_t^{1/3} + A_p^{1/3})\,\mathrm{fm}$ with $A_t = 12$, $A_p = 2$, $\pi R^2 \sim 400\,\mathrm{mb}$, a typical nuclear scale. Measured reaction cross sections can be larger (refractive/optical effects) or smaller (strong absorption and Q-value windows). Absolute normalisation is therefore a physics measurement, not a bookkeeping afterthought.

1.9 Further physics from the literature

Optical model and elastic scattering. Elastic scattering of nucleons is described by a complex optical potential whose imaginary part accounts for absorption into non-elastic channels. The resulting diffraction patterns and reaction cross sections connect to the total cross section via the optical theorem [6, 14, 2].

Optical theorem and unitarity. For wave number k, the forward elastic amplitude fixes the total loss of incident flux,

$$\sigma_{\mathrm{tot}} = \frac{4\pi}{k}\,\mathrm{Im}\, f(\theta = 0).$$

This is not a geometrical identity; it follows from probability conservation of the scattering matrix. The imaginary optical potential transfers flux from the explicitly treated elastic channel into all unresolved reaction channels.

DWBA for transfer. Direct stripping and pickup are analysed with the distorted-wave Born approximation (DWBA). Angular distributions determine the transferred orbital angular momentum ℓ; spectroscopic factors measure single-particle occupation relative to a pure shell-model configuration [6, 14].

Hauser–Feshbach theory. Statistical CN decay is computed with Hauser–Feshbach theory: transmission coefficients for all open channels, spin and parity conservation, and level densities. Bohr independence is built in by construction [6, 1]. Its predictions inherit uncertainties from optical potentials, level densities, gamma-strength functions, discrete-level schemes, and width-fluctuation corrections. Varying only one ingredient while holding the others fixed does not provide a complete model uncertainty; yield comparisons should distinguish experimental normalization errors from these correlated theory systematics.

What the mechanism labels do and do not mean. "Direct", "pre-equilibrium", and "compound" are dynamical limits, not three mutually exclusive final-state labels. The same measured channel can receive coherent direct and resonant amplitudes. A smooth forward component, an evaporation-like energy spectrum, and narrow fluctuations in an excitation function are therefore complementary evidence, rather than infallible one-feature classifiers. This distinction follows the presentation in the open H. C. Verma nuclear-reaction lectures [32].

Heavy-ion reactions. Heavy projectiles open fusion, deep-inelastic scattering, and multi-nucleon transfer. Timescales and angular distributions again separate quasi-elastic direct processes from long-lived fused systems [14, 2].

Reading guide

Krane [6] Ch. 11–12 (reactions, compound nucleus, direct reactions); Dunlap [1] (cross sections and experimental methods); Basdevant [14] (mechanisms); Demtröder [2] (accelerators and detectors); Verma [32], Nuclear Reaction Parts 1–3 (open lecture sequence). Ghoshal's classic comparison is [37]; see also the reaction chapters of Krane.

1.9.1 Quantitative direct versus compound discrimination

Direct stripping (d, p) on a target of mass A at beam energy $E_d \sim 10$–$20\,\mathrm{MeV}$ typically peaks in cross section near $\theta \sim 0^\circ$ with a characteristic diffraction pattern set by transferred ℓ. The differential cross section at the peak is often 0.1–10 mb/sr, while compound-nucleus background at the same angle may be ~ 0.01 mb/sr [6, 37]. The ratio of forward peak to isotropic background is a practical discriminator: direct reactions carry angular information; compound reactions average it away [14, 2].

Geometric versus measured reaction cross section

For $^{12}\mathrm{C} + ^{12}\mathrm{C}$ at $E_{\mathrm{CM}} \approx 5\,\mathrm{MeV}$, $\sigma_{\mathrm{geom}} \approx 850\,\mathrm{mb}$ but measured fusion cross sections are ~ 1–$10\,\mathrm{mb}$ because of Coulomb tunneling and angular-momentum filtering [6]. At neutron energies near 1 MeV on $^{238}\mathrm{U}$, $\sigma_{\mathrm{reaction}}$ can approach hundreds of barns, comparable to πR^2 for $R \approx 7\,\mathrm{fm}$, because the Coulomb barrier is absent [35, 6].

1.9.2 From direct reactions to kinematics and fission

Transfer reactions determine Q-values and excitation energies through two-body kinematics (Lecture 22). Stripping on fissile targets populates states that decay by fission when $E^* > B_f$ (Lecture 23). Knockout reactions on radioactive beams test the same single-particle overlap that preformation factors encode in α decay (Lectures 16–17) [51, 6]. Hauser–Feshbach compound decay feeds γ cascades analysed with multipole tools from Lecture 20.

Remark

The optical theorem links forward elastic scattering to the total cross section. Absorptive imaginary potentials that describe compound-nucleus formation therefore appear already in elastic channel analyses, connecting reaction cross sections to the same flux-conservation

logic used in decay widths [6, 14].

1.9.3 From stripping to fissile breeding

Neutron transfer and capture reactions on fertile ^{238}U populate ^{239}U, which β-decays to fissile ^{239}Pu (Lecture 24) [6, 35]. The (d, p) reaction on actinide targets is used to map single-particle states that also control α-decay preformation (Lectures 16–17) [51]. Geometric cross sections set the scale for neutron absorption in reactors; direct and compound mechanisms determine how much of that flux goes into useful channels versus background [1, 37].

1.9.4 Charge exchange and β strength in reactions

Charge-exchange reactions probe Gamow–Teller strength complementary to β decay (Lecture 19) [14, 51]. Transfer reactions on radioactive beams map single-particle occupancies that also control α-decay preformation (Lectures 16–17). The geometric cross section sets the overall flux; direct versus compound mechanisms determine whether angular distributions carry structural information or are washed out by statistical decay [6, 37]. Hauser–Feshbach theory connects compound cross sections to γ-cascade multipolarities (Lecture 20) through level densities and transmission coefficients [1, 6].

1.9.5 Hauser–Feshbach and the compound-nucleus limit

Hauser–Feshbach theory computes compound-nucleus decay as a statistical balance among open channels weighted by transmission coefficients and level densities [6, 1]. Bohr independence (decay independent of formation) is built into the theory by construction. Modern applications inherit uncertainties from optical potentials, γ-strength functions, and level-density models [51, 37]. The lecture distinction between direct (peripheral, angular-structure-rich) and compound (near-isotropic, energy-averaged) mechanisms remains the organising principle for interpreting rare-isotope reaction data at FRIB and comparable facilities [52, 6].

1.10 Deeper reading: direct versus compound and geometric scales

Direct reactions are peripheral and angular-structure-rich; compound reactions are energy-averaged and closer to isotropic after many intermediate-state scramble. Ghoshal-type tests illustrate compound formation; DWBA analyses of (d, p) illustrate direct transfer. Geometric cross sections πR^2 set the scale, but absolute spectroscopic factors inherit optical-potential uncertainties.

Rare-isotope beams amplify those issues: elastic data for exotic projectiles are sparse, so Bayesian optical potentials and continuum coupling matter. Classify any published angular distribution before trusting a quoted spectroscopic factor. Lectures 22's kinematics then tell you where to place detectors; Lecture 10's scattering theory tells you what the distorted waves mean.

entrangling structure and reaction

A measured differential cross section equals a structure factor times a reaction factor (schematically). Changing the optical potential changes the reaction factor and thus the extracted structure. Publish both or publish neither as a precision claim. Coupled-channels analyses that include target excitation blur the simple direct/compound dichotomy but still begin from Lecture 21's classification.

Charge exchange

Charge-exchange reactions map Gamow–Teller strength relevant to β decay and to astrophysical electron capture. Their interpretation reuses Lectures 14 and 19 operator themes inside a reaction framework from this chapter.

Classification drill

Find one published (d, p) angular distribution on a closed-shell target and one compound-nucleus excitation function. Write three bullets for each: angular shape, energy dependence, and what structure quantity (if any) was extracted. Then estimate πR^2 and compare with the magnitude of the reported cross section.

Discuss how continuum coupling and core excitation modify DWBA for exotic beams. The goal is not to run a coupled-channels code in this course, but to read a modern reaction paper without confusing a fitted spectroscopic factor with a pure shell-model occupation. Lectures 10 and 22 supply the scattering and kinematic prerequisites for that reading.

Reactions entangle structure with mechanism. Direct versus compound is the first cut; optical-model uncertainty is the modern second cut.

In practice, rework one numerical estimate from the lecture with a different parameter set and compare the shift to the quoted experimental uncertainty. If the shift exceeds the uncertainty, the estimate is teaching a scale, not delivering a fit. That distinction keeps theoretical cartoons honest when they sit beside evaluated data tables and modern many-body calculations. Along the course arc, write one sentence linking this chapter backward and one forward: the discipline of those two sentences is as important as any single formula. Examination problems rarely ask for a literature review, but they do ask for the scale argument that literature reviews presuppose.

Synthesis problem

Write a half-page note that (i) restates the chapter's central scale or selection rule in one equation, (ii) evaluates it numerically for one concrete nucleus or energy, and (iii) names the neighbouring lecture that uses the result. Keep the note free of research-frontier speculation; the goal is fluency with the lecture physics itself. If an assumption fails (Born approximation, spherical mean field, allowed transition, one-dimensional barrier), state the failure mode in a final sentence. That habit converts passive reading into examination-ready understanding and makes the later research-frontier box read as an extension rather than a replacement.

Research frontier: rare-isotope reactions and student projects

Direct and compound reactions of Lecture 21 are the workhorses of structure studies with radioactive beams. Transfer, knockout, and charge-exchange reactions at FRIB, FAIR, RIKEN, and TRIUMF map spectroscopic factors and Gamow–Teller strength far from stability; theory must treat continuum and core excitation to interpret the cross sections [51, 52]. Classic compound-nucleus tests such as Ghoshal's still illustrate the mechanism, but modern analyses include uncertainty quantification of optical potentials and level densities [37]. Open questions include the quenching of spectroscopic factors relative to independent-particle estimates, the validity of sudden approximations in knockout, and how to propagate optical-model uncertainties into extracted structure quantities. The lecture distinction between direct (peripheral, angular-structure-rich) and compound (near-isotropic, energy-averaged) mechanisms remains the organising principle for reading modern papers.

A recurring pitfall is to treat a DWBA spectroscopic factor as a pure structure number. Modern analyses vary optical potentials within uncertainty bands and report the induced spread. Student projects that repeat a published angular-distribution fit with two optical-potential families learn that lesson quantitatively.

The lecture direct-versus-compound classification remains the first cut before those uncertainty bands are interpreted.

Facility white papers list transfer, knockout, and charge exchange among the first experiments for new beam species for exactly this experimental reason.

Student directions. (1) Classification exercise: classify a published (d, p) study as direct or compound using angular distributions. (2) Scale estimate: compute a geometric cross section and compare with a measured reaction cross section at Coulomb-barrier energy. (3) Methods project: outline extracting a spectroscopic factor from published angular-distribution data with a DWBA code.

1.11 Problems with solutions

Problem 21.1: Differential cross section from counts

A beam of flux density $\Phi = 2.0 \times 10^{10}\,\mathrm{cm^{-2}\,s^{-1}}$ illuminates $N_t = 1.5 \times 10^{19}$ target nuclei. In $\Delta t = 100\,\mathrm{s}$, a detector with $\Delta\Omega = 5.0 \times 10^{-3}\,\mathrm{sr}$ records $N = 3.0 \times 10^{4}$ product particles (assume $\mathrm{d}\sigma/\mathrm{d}\Omega$ constant over the detector). Find $\mathrm{d}\sigma/\mathrm{d}\Omega$ in mb/sr [6, 1].

Solution 21.1

From $\mathrm{d}\dot{N} = \Phi N_t(\mathrm{d}\sigma/\mathrm{d}\Omega)\mathrm{d}\Omega$, integrated over the run,

$$N = \Phi N_t \frac{\mathrm{d}\sigma}{\mathrm{d}\Omega}\Delta\Omega\,\Delta t.$$

$$\begin{aligned}\frac{\mathrm{d}\sigma}{\mathrm{d}\Omega} &= \frac{N}{\Phi N_t\,\Delta\Omega\,\Delta t}\\ &= \frac{3.0\times10^{4}}{(2.0\times10^{10})(1.5\times10^{19})(5.0\times10^{-3})(100)}\\ &= \frac{3.0\times10^{4}}{1.5\times10^{30}}\\ &= 2.0\times10^{-26}\,\mathrm{cm}^2/\mathrm{sr}.\end{aligned}$$

Since $1\,\mathrm{b}=10^{-24}\,\mathrm{cm}^2$,

$$\frac{\mathrm{d}\sigma}{\mathrm{d}\Omega} = 0.020\,\mathrm{b/sr} = 20\,\mathrm{mb/sr}.$$

Problem 21.2: Areal density

A gold foil ($A=197$, density $\rho=19.3\,\mathrm{g\,cm^{-3}}$) has thickness $t=2.0\,\mu\mathrm{m}$. Estimate the areal density $n_a=nt$ in nuclei per cm^2. Use $N_A=6.02\times10^{23}\,\mathrm{mol^{-1}}$ [1].

Solution 21.2

Number density

$$n=\frac{\rho N_A}{A}=\frac{19.3\times6.02\times10^{23}}{197}=5.90\times10^{22}\,\mathrm{cm^{-3}}.$$

$$t=2.0\times10^{-4}\,\mathrm{cm},\qquad n_a=nt=1.18\times10^{19}\,\mathrm{cm^{-2}}.$$

Problem 21.3: Lab to CM energy

A $12.0\,\mathrm{MeV}$ proton beam strikes a stationary $^{12}\mathrm{C}$ target. Find E_{cm}. What fraction of E_{lab} is unavailable for excitation? [6]

Solution 21.3

$$E_{\mathrm{cm}}=\frac{m_C}{m_p+m_C}E_{\mathrm{lab}}\approx\frac{12}{13}\times12.0\,\mathrm{MeV}=11.08\,\mathrm{MeV}.$$

Unavailable fraction (CM motion):

$$\frac{m_p}{m_p+m_C}=\frac{1}{13}\approx7.7\%.$$

Problem 21.4: Coulomb barrier estimate

Estimate V_C at contact for $\alpha+{}^{208}\mathrm{Pb}$ using $R=1.2(A_\alpha^{1/3}+A_{\mathrm{Pb}}^{1/3})\,\mathrm{fm}$ and $e^2/(4\pi\varepsilon_0)=1.44\,\mathrm{MeV\cdot fm}$ [6, 1].

Solution 21.4

$$R = 1.2(4^{1/3} + 208^{1/3}) = 1.2(1.59 + 5.92) = 9.01\,\text{fm}.$$

$$V_C = \frac{(2)(82)(1.44)}{9.01} = \frac{236.2}{9.01} \approx 26.2\,\text{MeV}.$$

An α beam well below $\sim 26\,\text{MeV}$ (lab, with CM correction) interacts mainly by Coulomb scattering unless it tunnels.

Problem 21.5: Direct transit time

Estimate the transit time of a 20 MeV proton across a nucleus of diameter 10 fm. Use non-relativistic kinematics with $m_p c^2 \approx 938\,\text{MeV}$ [6].

Solution 21.5

$$\tfrac{1}{2}mv^2 = 20\,\text{MeV} \quad \Rightarrow \quad \frac{v}{c} = \sqrt{\frac{2K}{mc^2}} = \sqrt{\frac{40}{938}} \approx 0.206.$$

$$t = \frac{10\,\text{fm}}{0.206\,c} = \frac{10 \times 10^{-15}\,\text{m}}{0.206 \times 3.00 \times 10^{8}\,\text{m s}^{-1}} \approx 1.6 \times 10^{-22}\,\text{s}.$$

This matches the direct-reaction timescale $\sim 10^{-22}\,\text{s}$.

Problem 21.6: Classify the process

Classify each as elastic, inelastic, stripping, pickup, or capture [6, 1]:

(a) $^{40}\text{Ca}(p,p)^{40}\text{Ca}$ (g.s. to g.s.);

(b) $^{40}\text{Ca}(p,p')^{40}\text{Ca}^*$;

(c) $^{40}\text{Ca}(d,p)^{41}\text{Ca}$;

(d) $^{40}\text{Ca}(p,d)^{39}\text{Ca}$;

(e) $^{40}\text{Ca}(n,\gamma)^{41}\text{Ca}$.

Solution 21.6

(a) Elastic scattering.
(b) Inelastic scattering.
(c) Stripping (deuteron loses a neutron).
(d) Pickup (proton gains a neutron).
(e) Radiative capture.

Problem 21.7: Bohr independence

Two entrance channels form the same compound nucleus C^* at the same excitation energy and spin. What does Bohr independence predict for the relative yields of two exit channels $b_1 + B_1$ and $b_2 + B_2$? Why must laboratory energies differ for $p + A$ versus $\alpha + A'$? [6]

Solution 21.7

Independence predicts that branching ratios (relative partial widths) of C^* are the same regardless of entrance channel. Absolute cross sections still contain an entrance formation factor, but excitation functions for a given exit channel should match when plotted versus excitation energy of C^*.

Laboratory energies differ because the Q-value for forming C and the mass ratios in $E_{\mathrm{cm}} = m_A K_a/(m_a + m_A)$ differ for (p, A) and (α, A'). Matching ΔE requires different K_a scales (Ghoshal plot with two energy axes).

Problem 21.8: Luminosity, efficiency, and target attenuation

A $5.0 \times 10^8\,\mathrm{s}^{-1}$ beam crosses a foil of areal density $n_a = 2.0 \times 10^{18}\,\mathrm{cm}^{-2}$. A channel has $\sigma_c = 80\,\mathrm{mb}$, and the apparatus accepts 2.0% of its products with 65% net efficiency. (a) Find the luminosity. (b) Find the observed rate. (c) If the total interaction cross section is 1.5 b, check the thin-target approximation [6, 1].

Solution 21.8

Step 1: luminosity.

$$\mathcal{L} = \dot{N}_a n_a = (5.0 \times 10^8)(2.0 \times 10^{18}) = 1.0 \times 10^{27}\,\mathrm{cm}^{-2}\,\mathrm{s}^{-1}.$$

Step 2: produced and observed rates. Since $80\,\mathrm{mb} = 8.0 \times 10^{-26}\,\mathrm{cm}^2$,

$$\dot{N}_c = \mathcal{L}\sigma_c = 80\,\mathrm{s}^{-1}, \qquad \dot{N}_{\mathrm{obs}} = 80(0.020)(0.65) = 1.04\,\mathrm{s}^{-1}.$$

Step 3: attenuation test.

$$\tau = n_a \sigma_{\mathrm{tot}} = (2.0 \times 10^{18})(1.5 \times 10^{-24}) = 3.0 \times 10^{-6}, \qquad P_{\mathrm{int}} = 1 - e^{-\tau} \simeq \tau.$$

The quadratic correction is of relative order $\tau/2$, so attenuation is negligible and the thin-target yield formula is justified.

Problem 21.9: Yield with propagated uncertainty

A thin-target run has $\dot{N}_a = (5.00 \pm 0.10) \times 10^8\,\mathrm{s}^{-1}$, $n_a = (2.00 \pm 0.06) \times 10^{18}\,\mathrm{cm}^{-2}$, efficiency $\epsilon = 0.650 \pm 0.020$, live time $T = 1000\,\mathrm{s}$, and $\sigma = 80.0\,\mathrm{mb}$. Find the expected count and its uncertainty, assuming independent inputs and negligible counting fluctuation [6, 1].

Solution 21.9

$$N = \dot{N}_a n_a \sigma \epsilon T = (5.00 \times 10^8)(2.00 \times 10^{18})(8.00 \times 10^{-26})(0.650)(1000) = 5.20 \times 10^4.$$

For a product of independent quantities,

$$\left(\frac{u_N}{N}\right)^2 = \left(\frac{0.10}{5.00}\right)^2 + \left(\frac{0.06}{2.00}\right)^2 + \left(\frac{0.020}{0.650}\right)^2 = 0.00225.$$

Thus $u_N/N = 0.0474$, $u_N = 2.47 \times 10^3$, and $N = (5.20 \pm 0.25) \times 10^4$. A real extraction would also include background, solid-angle, dead-time, and cross-section-model systematics.

Problem 21.10: When Hauser–Feshbach is unreliable

For each case state whether a basic Hauser–Feshbach average is well motivated: (a) hundreds of overlapping compound levels in each J^π bin; (b) one isolated near-threshold resonance; (c) a strong forward direct-transfer amplitude in the same exit channel. Name the missing physics where needed [6, 1].

Solution 21.10

(a) is the intended statistical limit, provided all important transmission coefficients and level densities are included. (b) requires an explicit Breit–Wigner or R-matrix treatment and may need width-fluctuation corrections. (c) requires a direct-reaction amplitude and, where coherent, its interference with the compound amplitude. The labels describe dynamical limits, not mutually exclusive measured channels.

Bibliography

[1] R. A. Dunlap, *An Introduction to the Physics of Nuclei and Particles* (2nd ed.), IOP Publishing, Bristol (2023), DOI: 10.1088/978-0-7503-6094-4, Ch. 3 (Nuclear composition and size).

[2] W. Demtröder, *Nuclear and Particle Physics*, Undergraduate Lecture Notes in Physics, Springer, Cham (2023).

[3] S. Petrera, *Problems and Solutions in Nuclear and Particle Physics*, UNITEXT for Physics, Springer, Cham (2019).

[4] F. Terranova, *A Modern Primer in Particle and Nuclear Physics*, Oxford University Press (2021).

[5] S. D'Auria, *Introduction to Nuclear and Particle Physics*, Undergraduate Lecture Notes in Physics, Springer, Cham (2018).

[6] K. S. Krane, *Introductory Nuclear Physics*, Wiley, New York (1988).

[7] R. Hofstadter, "Electron scattering and nuclear structure," Rev. Mod. Phys. **28**, 214 (1956).

[8] H. F. Ehrenberg, R. Hofstadter, U. Meyer-Berkhout, D. G. Ravenhall, and S. E. Sobottka, "High-Energy Electron Scattering and the Charge Distribution of Carbon-12 and Oxygen-16," Phys. Rev. **113**, 666 (1959).

[9] H. Yukawa, "On the interaction of elementary particles. I," Proc. Phys.-Math. Soc. Japan **17**, 48 (1935).

[10] R. D. Woods and D. S. Saxon, "Diffuse surface optical model for nucleon-nuclei scattering," Phys. Rev. **95**, 577 (1954).

[11] H. G. J. Moseley, "The high-frequency spectra of the elements," Phil. Mag. **26**, 1024 (1913); **27**, 703 (1914).

[12] C. F. von Weizsäcker, "Zur Theorie der Kernmassen," Z. Phys. **96**, 431 (1935).

[13] P. Cappellaro, *Introduction to Applied Nuclear Physics* (MIT OpenCourseWare / LibreTexts), CC BY-NC-SA 4.0.

[14] J.-L. Basdevant, J. Rich, and M. Spiro, *Fundamentals in Nuclear Physics: From Nuclear Structure to Cosmology*, Springer, New York (2005).

[15] D. Tong, *Particle Physics*, Lecture notes (University of Cambridge / CERN school notes).

[16] M. G. Mayer, "On closed shells in nuclei. II," Phys. Rev. **75**, 1969 (1949).

[17] O. Haxel, J. H. D. Jensen, and H. E. Suess, "On the "magic numbers" in nuclear structure," Phys. Rev. **75**, 1766 (1949).

[18] T. Schmidt, "Über die magnetischen Momente der Atomkerne," Z. Phys. **106**, 358 (1937).

[19] L. W. Nordheim, "On spins, moments, and shells in nuclei," Phys. Rev. **78**, 294 (1950).

[20] Evaluated Nuclear Structure Data File (ENSDF), National Nuclear Data Center, Brookhaven National Laboratory, `https://www.nndc.bnl.gov/ensdf/`.

[21] NuDat 3, National Nuclear Data Center, Brookhaven National Laboratory, `https://www.nndc.bnl.gov/nudat3/`.

[22] N. J. Stone, "Table of nuclear magnetic dipole and electric quadrupole moments," At. Data Nucl. Data Tables **90**, 75 (2005); updated compilations at NNDC.

[23] W. N. Cottingham and D. A. Greenwood, *An Introduction to Nuclear Physics* (2nd ed.), Cambridge University Press, Cambridge (2001).

[24] H. Geiger and J. M. Nuttall, "The ranges of the α particles from the radioactive substances," Phil. Mag. **22**, 613 (1911).

[25] G. Gamow, "Zur Quantentheorie des Atomkernes," Z. Phys. **51**, 204 (1928).

[26] R. W. Gurney and E. U. Condon, "Wave mechanics and radioactive disintegration," Nature **122**, 439 (1928); Phys. Rev. **33**, 127 (1929).

[27] M. Wang, W. J. Huang, F. G. Kondev, G. Audi, and S. Naimi, "The AME 2020 atomic mass evaluation (II). Tables, graphs and references," Chin. Phys. C **45**, 030003 (2021).

[28] Laboratoire National Henri Becquerel (LNHB), Recommended decay data, `http://www.lnhb.fr/nuclear-data/nuclear-data-table/`.

[29] L. M. Langer, R. D. Moffat, and H. C. Price, Jr., "Low energy beta-ray spectra: P^{32} and Cu^{64}," Phys. Rev. **76**, 1725 (1949).

[30] L. M. Langer and H. C. Price, Jr., "Shapes of the beta-spectra of the forbidden transitions of Sb^{124}, Rb^{86}, Sr^{89}, Y^{91}, and Cs^{137}," Phys. Rev. **75**, 1769 (1949).

[31] D. C. Camp and L. M. Langer, "The shape of the ^{66}Ga positron spectrum and the contribution from $0^+ \to 0^+$ transitions," Phys. Rev. **129**, 1782 (1963).

[32] H. C. Verma, *Nuclear Physics: Fundamentals and Applications*, NPTEL/IIT Kanpur lecture series, `https://hcverma.in/ncl_phy_lectures`.

[33] International Atomic Energy Agency, *LiveChart of Nuclides*, evaluated structure, decay, reaction, and fission-yield data, `https://www-nds.iaea.org/relnsd/vcharthtml/VChartHTML.html`.

[34] T. Kibédi, T. W. Burrows, M. B. Trzhaskovskaya, P. M. Davidson, and C. W. Nestor, Jr., "Evaluation of theoretical conversion coefficients using BrIcc," Nucl. Instrum. Methods Phys. Res. A **589**, 202 (2008), DOI: 10.1016/j.nima.2008.02.051.

[35] D. A. Brown *et al.*, "ENDF/B-VIII.0: The 8th major release of the nuclear reaction data library with CIELO-project cross sections, new standards and thermal scattering data," Nucl. Data Sheets **148**, 1 (2018), DOI: 10.1016/j.nds.2018.02.001.

[36] B. Acharya *et al.*, "Solar fusion III: New data and theory for hydrogen-burning stars," Rev. Mod. Phys. **97**, 035002 (2025), DOI: 10.1103/8lm7-gs18.

[37] S. N. Ghoshal, "An experimental verification of the theory of compound nucleus," Phys. Rev. **80**, 939 (1950), DOI: 10.1103/PhysRev.80.939.

[38] D. Adhikari *et al.* (PREX Collaboration), "Accurate determination of the neutron skin thickness of ^{208}Pb through parity-violation in electron scattering," Phys. Rev. Lett. **126**, 172502 (2021), DOI: 10.1103/PhysRevLett.126.172502.

[39] B. T. Reed, F. J. Fattoyev, C. J. Horowitz, and J. Piekarewicz, "Implications of PREX-II on the equation of state of neutron-rich matter," Phys. Rev. Lett. **126**, 172503 (2021), DOI: 10.1103/PhysRevLett.126.172503.

[40] B. Hu *et al.*, "Ab initio predictions link the neutron skin of ^{208}Pb to nuclear forces," Nature Phys. **18**, 1196 (2022), DOI: 10.1038/s41567-022-01715-8.

[41] E. Epelbaum, H.-W. Hammer, and U.-G. Meißner, "Modern theory of nuclear forces," Rev. Mod. Phys. **81**, 1773 (2009), DOI: 10.1103/RevModPhys.81.1773.

[42] H.-W. Hammer, S. König, and U. van Kolck, "Nuclear effective field theory: Status and perspectives," Rev. Mod. Phys. **92**, 025004 (2020), DOI: 10.1103/RevModPhys.92.025004.

[43] T. Otsuka, A. Gade, O. Sorlin, T. Suzuki, and Y. Utsuno, "Evolution of shell structure in exotic nuclei," Rev. Mod. Phys. **92**, 015002 (2020), DOI: 10.1103/RevModPhys.92.015002.

[44] H. Hergert, S. K. Bogner, T. D. Morris, A. Schwenk, and K. Tsukiyama, "The in-medium similarity renormalization group: A novel ab initio method for nuclei," Phys. Rep. **621**, 165 (2016), DOI: 10.1016/j.physrep.2015.12.007.

[45] J. M. Lattimer and M. Prakash, "The equation of state of hot, dense matter and neutron stars," Phys. Rep. **621**, 127 (2016), DOI: 10.1016/j.physrep.2015.12.005.

[46] J. M. Lattimer, "Neutron stars and the nuclear matter equation of state," Annu. Rev. Nucl. Part. Sci. **71**, 433 (2021), DOI: 10.1146/annurev-nucl-102419-124827.

[47] B. P. Abbott *et al.* (LIGO Scientific Collaboration and Virgo Collaboration), "GW170817: Observation of gravitational waves from a binary neutron star inspiral," Phys. Rev. Lett. **119**, 161101 (2017), DOI: 10.1103/PhysRevLett.119.161101.

[48] M. J. Dolinski, A. W. P. Poon, and W. Rodejohann, "Neutrinoless double-beta decay: Status and prospects," Annu. Rev. Nucl. Part. Sci. **69**, 219 (2019), DOI: 10.1146/annurev-nucl-101918-023407.

[49] M. Agostini, G. Benato, J. A. Detwiler, J. Menéndez, and F. Vissani, "Toward the discovery of matter creation with neutrinoless $\beta\beta$ decay," Rev. Mod. Phys. **95**, 025002 (2023), DOI: 10.1103/RevModPhys.95.025002.

[50] P. Gysbers *et al.*, "Discrepancy between experimental and theoretical β-decay rates resolved from first principles," Nature Phys. **15**, 428 (2019), DOI: 10.1038/s41567-019-0450-7.

[51] H. L. Crawford, K. Fossez, S. König, and A. Spyrou, "A vision for the science of rare isotopes," Annu. Rev. Nucl. Part. Sci. **74**, 141 (2024), DOI: 10.1146/annurev-nucl-121423-091501.

[52] Nuclear Science Advisory Committee, *A New Era of Discovery: The 2023 Long Range Plan for Nuclear Science*, U.S. Department of Energy and National Science Foundation (2023), `https://nuclearsciencefuture.org/`.

[53] S. A. Giuliani, Z. Matheson, W. Nazarewicz, E. Olsen, P.-G. Reinhard, J. Sadhukhan, B. Schuetrumpf, N. Schunck, and P. Schwerdtfeger, "Colloquium: Superheavy elements: Oganesson and beyond," Rev. Mod. Phys. **91**, 011001 (2019), DOI: 10.1103/RevModPhys.91.011001.

[54] N. Schunck and D. Regnier, "Theory of nuclear fission," Prog. Part. Nucl. Phys. **125**, 103963 (2022), DOI: 10.1016/j.ppnp.2022.103963.

[55] I. Counts, J. Hur, D. P. L. Aude Craik, H. Jeon, C. Leung, J. C. Berengut, A. Geddes, A. Kawasaki, W. Jhe, and V. Vuletić, "Evidence for nonlinear isotope shift in Yb^+ search for new boson," Phys. Rev. Lett. **125**, 123002 (2020), DOI: 10.1103/PhysRevLett.125.123002.

[56] I. Angeli and K. P. Marinova, "Table of experimental nuclear ground state charge radii: An update," At. Data Nucl. Data Tables **99**, 69 (2013), DOI: 10.1016/j.adt.2011.12.006.

[57] S. Kraemer *et al.*, "Observation of the radiative decay of the ^{229}Th nuclear clock isomer," Nature **617**, 706 (2023), DOI: 10.1038/s41586-023-05894-z.